J Mater Sci (2008) 43:6435–6440
DOI 10.1007/s10853-008-2631-0

Pulsed electric current sintering of electrically conductive ceramics

K. Vanmeensel · S. G. Huang · A. Laptev · S. A. Salehi · A. K. Swarnakar · O. Van der Biest · J. Vleugels

Received: 29 November 2007 / Accepted: 31 March 2008 / Published online: 9 July 2008

Abstract The processing of yttria-stabilised zirconia (Y-ZrO_2)-based ceramic nanocomposites by means of pulsed electric current sintering (PECS) is described. A nanometer-sized electrically conductive secondary TiCN phase was added to the insulating zirconia matrix in order to make the composite electrically conductive. The paper focuses on the importance of processing conditions and highlights the benefits of the PECS method as compared to more traditional hot pressing. The mechanical and microstructural properties of the ZrO_2–TiCN composites have been determined, and the benefits of using an electrical current to densify these composites were explained in terms of the evolution of the electrical properties of the densifying powder compact.

Introduction

During the last decade, the applicability of zirconia to induce toughening by the stress-induced transformation of the tetragonal to monoclinic ZrO_2 phase in the stress field of propagating cracks, a phenomenon known as transformation toughening [1, 2], has been intensively investigated. Recent developments in zirconia composites are focused not only on the improvement of toughness, strength and hardness, but also on the possibility for mass production and manufacturing cost reduction. A successful approach is to incorporate electrically conductive reinforcements such as TiB_2 [3], WC [4], ZrB_2 [5], TiC [6], TiCN [7], and TiN [8] into the zirconia matrix. The incorporation of a certain amount of these conductive reinforcements makes the composite electrically conductive enough to be machine able by electrical discharge machining (EDM), thus avoiding the expensive cutting and grinding operation for component shaping.

However, only few investigations exist on the production of bulk ceramic nanocomposites that are electrically conductive [9–12] due to the limited availability of nanometer-sized, electrically conductive ceramic particles [13] and the difficulty to maintain the originally available nanostructure in the final densified bulk component [14].

Therefore, this study focuses on the processing of nanometer-sized ZrO_2–$TiC_{0.5}N_{0.5}$ (60/40) (vol%) bulk ceramic components. The importance of the mixing method is highlighted, hereby focussing on the dispersion of the secondary TiCN phase particles in the Y-ZrO_2 matrix. In order to overcome the problem of grain growth and coarsening of the microstructure [15–17] during densification of the mixed composite powder compacts, the pulsed electric current sintering (PECS) technique, also known as spark plasma sintering (SPS) or field-assisted sintering technology (FAST), has been used, allowing the use of high heating and cooling rates as well as short dwell times.

Experimental procedures

The commercial nanopowders that have been used are yttria-free monoclinic ZrO_2 (Tosoh grade TZ-0, Tokyo,

K. Vanmeensel · S. G. Huang · S. A. Salehi · A. K. Swarnakar · O. Van der Biest · J. Vleugels (✉)
Department of Metallurgy and Materials Engineering (MTM), K.U.Leuven, Kasteelpark Arenberg 44, 3001 Heverlee (Leuven), Belgium
e-mail: jozef.vleugels@mtm.kuleuven.be

A. Laptev
Department of Mechanical Engineering, Donbass State Engineering Academy, Shkadinova 72, Kramatorsk 343913, Ukraine

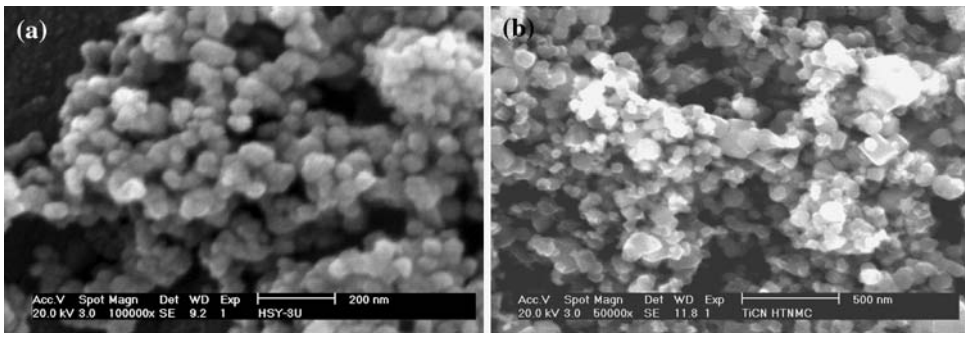

Fig. 1 SEM of the 3Y-ZrO_2 (**a**) and $TiC_{0.5}N_{0.5}$ (**b**) nanometer-sized starting powders

Japan), 3 mol% yttria-stabilised zirconia (Daiichi grade HSY-3U, Japan) and TiCN (HTNMC grade, Hebei Sinochem, China). The Y_2O_3 stabiliser content was adjusted by mixing the appropriate amounts of monoclinic and yttria-stabilised zirconia powder [18]. The morphology of the starting powders is shown in Fig. 1.

Two types of powder mixing/milling procedures have been used. At first, the powder mixtures were mixed in a multidirectional Turbula mixer (type T2A, Basel, Switzerland) in ethanol in a polyethylene container of 250 mL during 48 h at 60 rpm. 250-g zirconia milling balls (Tosoh grade TZ-3Y, Tokyo, Japan) with a diameter of 10 mm were added to the container to break the agglomerates in the starting powder and to enhance powder mixing. Secondly, the powder mixtures were bead milled (Dispermat SL, VMA Getzmann GmbH, Reichshof, Germany) in ethanol at 6,000 rpm for 2 h using 3Y-ZrO_2 beads with an average size of 0.4–0.7 mm. The ethanol was removed after mixing using a rotating evaporator.

The dry powder mixtures were sieved and inserted into a graphite die/punch set-up (inner diameter of 40 mm, outer diameter of 56 mm), as described elsewhere [19]. All samples were PECS (Type HP D 25/1, FCT Systeme, Rauenstein, Germany, equipped with a 250-kN uniaxial-press) in vacuum ($\sim$0.05 Pa) for 2 min at 1,400 °C under a load of 60 MPa, applying a heating rate of 50–200 °C/min. Hot pressing (HP) (W100/150-2200-50 LAX, FCT Systeme, Rauenstein, Germany) was performed in vacuum at 60 MPa and 1,400 °C, applying a maximum heating rate of 50 °C/min.

The density of the samples was measured in ethanol, according to the Archimedes method (BP210S balance, Sartorius AG, Germany). The Vickers hardness (HV_{10}) was measured on a hardness tester (Model FV-700, Future-Tech, Japan) with an indentation load of 98 N. The indentation toughness, K_{IC}, based on the crack length measurement of the radial crack pattern produced by Vickers HV_{10} indentations was calculated according to the formula of Anstis et al. [20]. The reported values are the average and standard deviations from at least ten indentations. The elastic modulus (E) was measured using the resonance frequency method [21]. The resonance frequency was measured by the impulse excitation technique (Model Grindo-Sonic, Lemmens N·V., Leuven, Belgium). X-ray diffraction (XRD) (Seifert 3003 T/T, Ahrensburg, Germany) analysis was used for phase identification and calculation of the transformability of the ZrO_2-based composites [22]. The 3-point flexural strength was measured (Instron 4467, PA**,** USA) on rectangular samples (25.0 × 5.4 × 2.1 mm^3), with a span length of 20 mm and a crosshead displacement of 0.2 mm/min. The reported values are the mean and standard deviation of five measurements. All sample surfaces were ground with a diamond grinding wheel (type MD4075B55, Wendt Boart, Brussels, Belgium) on a Jung grinding machine (JF415DS, Göppingen, Germany).

Results

Mechanical and microstructural characterisation

In order to investigate the influence of the mixing method on the microstructural homogeneity of the ZrO_2–TiCN (60/40) composites, powder mixtures obtained by multidirectional mixing and bead milling were PECS according to the temperature and pressure cycle as shown in Fig. 2.

The temperature was increased from room temperature to 450 °C, applying a constant voltage under a minimum pressure of 7 MPa. From 450 °C onwards, the thermal cycle was PID controlled using the preset temperature profile as shown in Fig. 2. At 450 °C, the temperature was

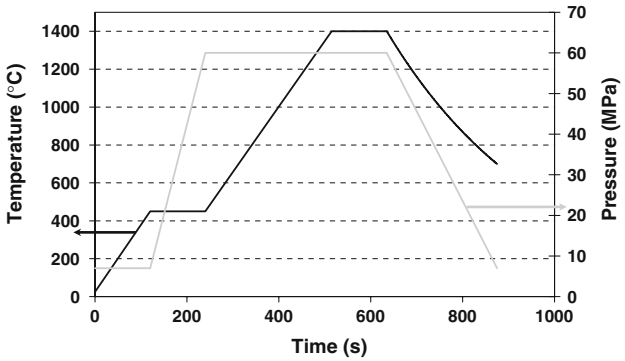

Fig. 2 PECS temperature and pressure cycle

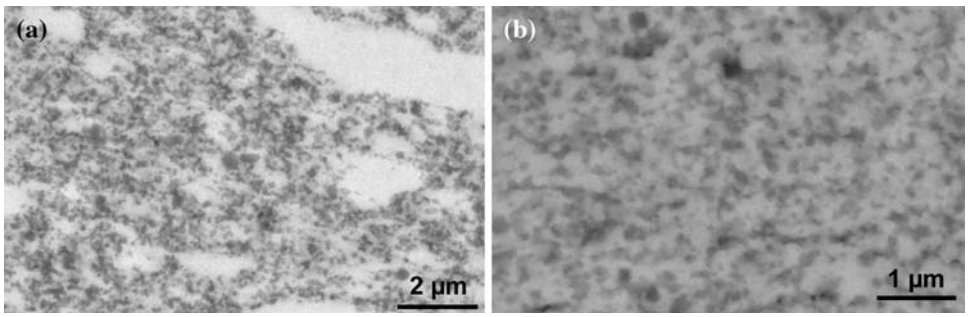

Fig. 3 Backscattered electron (BSE) micrographs of the multidirectionally mixed (**a**) and bead milled (**b**) powder-based ZrO_2–TiCN (60/40) composites, PECS for 2 min at 1,400 °C

dwelled for 2 min in order to increase the pressure to 60 MPa. From 450 to 1,400 °C, a fixed heating rate of 200 °C/min was applied, after which the temperature and pressure were dwelled for 2 min. Cooling was performed by switching off the pulsed current. The total cycle time was less than 20 min.

The microstructure of the PECS materials is shown in Fig. 3, clearly illustrating that bead milling allows to obtain a much more homogeneous microstructure than multidirectional mixing.

The measured density of the multidirectionally mixed and bead-milled powder-based ceramics was 96.8 and 97.1% of their theoretical density, respectively, using a theoretical density of 6.03 and 5.18 g/cm^3 for 3Y-ZrO_2 and $TiC_{0.5}N_{0.5}$. Since no porosity can be observed in Fig. 3a and b, it is reasonable to assume that the theoretical density of the $TiC_{0.5}N_{0.5}$ powder is decreased by the presence of the Ti_3O_5 impurity, as revealed by the XRD pattern of the $TiC_{0.5}N_{0.5}$ starting powder as shown in Fig. 4.

The composites were obtained by mixing 3Y-ZrO_2 and $TiC_{0.5}N_{0.5}$ starting powders. In order to improve the fracture toughness of zirconia ceramics, the overall yttria stabiliser content should be decreased [18].

The mechanical properties of the ZrO_2–TiCN (60/40) composites are summarised in Table 1 as a function of the overall yttria stabiliser content, together with those of a 2Y-ZrO_2 reference material, PECS under the same conditions. The fracture toughness and bending strength of the nanocomposites could be successfully improved by decreasing the yttria stabiliser content from 3 to 2 mol%. At a lower stabiliser content of 1.75 mol%, the density and all investigated properties were found to decrease again. Moreover, the properties of the 2 mol% yttria-stabilised ZrO_2–TiCN nanocomposite are superior to those of the 2Y-TZP ceramic. Very high fracture toughness could be obtained for the ZrO_2–$TiC_{0.5}N_{0.5}$ (60/40) nanocomposite with 2 mol% yttria stabiliser, as confirmed by the limited length of the propagating cracks originating from the corners of a Vickers hardness indentation (Fig. 5a). This proves that it is possible to increase the fracture toughness of the material, while maintaining the intrinsic nanostructure of the nanopowders when using fast densification by PECS, as shown in Fig. 5b.

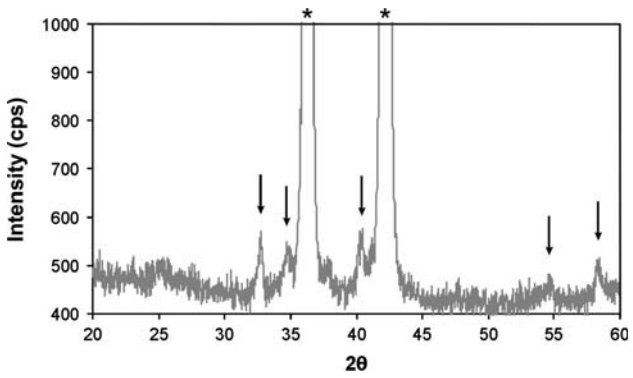

Fig. 4 Diffraction pattern of the $TiC_{0.5}N_{0.5}$ starting powder, revealing $TiC_{0.5}N_{0.5}$ (*) and Ti_3O_5 (↓)

Comparison of PECS and HP

In order to investigate the influence of the electrical current on the densification behaviour of the ZrO_2–TiCN (60/40) composite material, two experiments, applying similar pressures, temperatures, heating rates and dwell times, were performed, both in a traditional hot press with a graphite heating element and by means of PECS. Due to the limited heating rate of the hot press, the experiments were performed with a heating rate of 50 °C/min (Fig. 6a), using the same punch/die set-up. The thermal cycle in the hot press was calibrated by means of a thermocouple in the centre of the die/punch set-up. A previous investigation pointed out that the temperature of the sintering powder compact during PECS can be accurately controlled using a central pyrometer set-up [19]. Therefore, it can be stated that the temperature of the sintering powder compacts during HP and PECS are similar. The densification behaviour of the powder compact was extracted from the piston travel during the PECS and HP cycle. In both cases, blank runs were performed in order to correct for the thermal expansion of the different parts of the set-up, as shown for the HP experiment in Fig. 6b.

The densification behaviour of the ZrO_2–$TiC_{0.5}N_{0.5}$ (60/40) powder compact during both HP and PECS, using

Table 1 Mechanical properties of the PECS ZrO_2–$TiC_{0.5}N_{0.5}$ (60/40) composites as a function of the yttria stabiliser content

Y_2O_3 content (mol%)	Density (g/cm^3)	*E*-modulus (GPa)	Vickers hardness (kg/mm^2)	Fracture toughness (MPa $m^{1/2}$)	3-point bending strength (MPa)
3	5.52	233	1342 ± 27	4.8 ± 0.3	1201 ± 66
2.5	5.54	229	1333 ± 17	5.4 ± 0.4	1278 ± 80
2	5.57	232	1338 ± 30	9.2 ± 0.5	1303 ± 71
1.75	5.47	206	1190 ± 59	6.1 ± 0.4	788 ± 111
2Y-TZP[a]	6.00	207	1260 ± 11	7.2 ± 0.1	1167 ± 76

[a] Mechanical properties of a 2Y-TZP ceramic, PECS under the same conditions

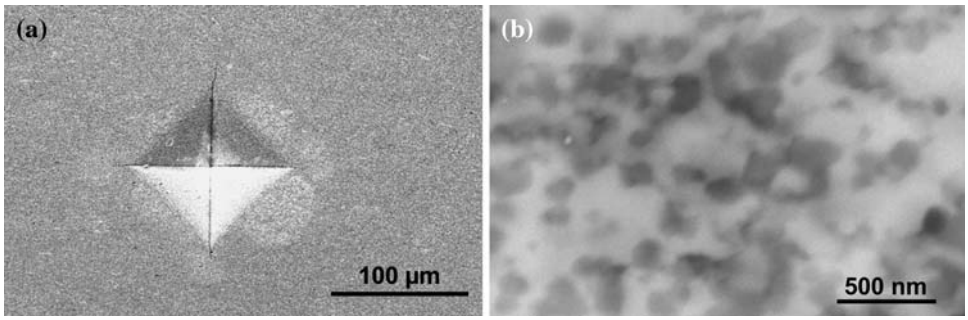

Fig. 5 BSE micrographs of the radial crack pattern around an HV_{10} Vickers indentation (**a**) and the microstructure (**b**) of the 2 mol% yttria-stabilised ZrO_2–TiCN (60/40) composite. White, Y-ZrO_2, Grey, $TiC_{0.5}N_{0.5}$

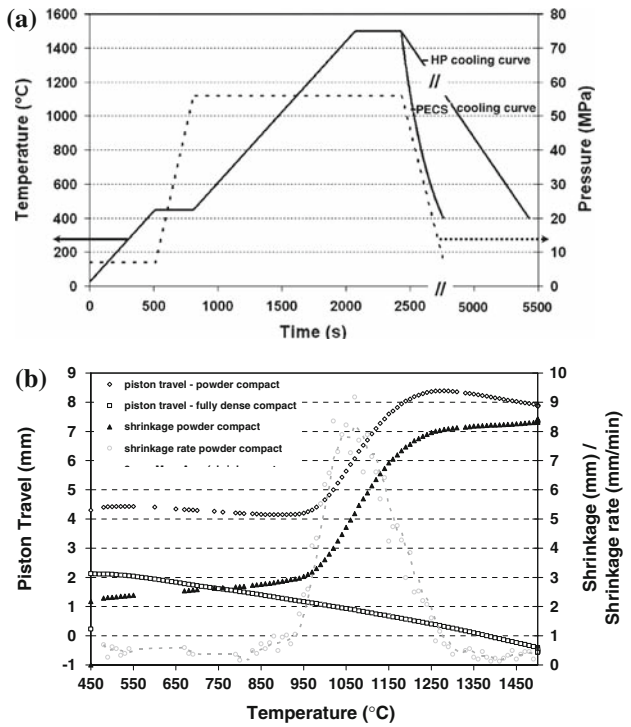

Fig. 6 Sintering cycle used to compare the densification behaviour of ZrO_2–$TiC_{0.5}N_{0.5}$ (60/40) powder compacts by PECS or HP (**a**) and the densification behaviour of the compact during HP as extracted from the corrected piston travel (**b**)

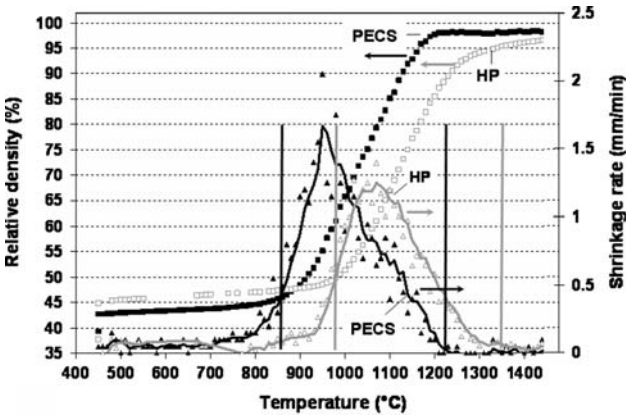

Fig. 7 Comparison of the relative density evolution of a sintering ZrO_2–$TiC_{0.5}N_{0.5}$ (60/40) powder compact during HP (□) and PECS (■), following the sintering cycle shown in Fig. 6a. The calculated shrinkage rates based on the experimentally determined piston travel curves are shown as well in case of HP (△) and PECS (▲). The vertical black and grey lines indicate the intermediate sintering stage during PECS and HP, respectively

the sintering cycle as shown in Fig. 6a, is compared in Fig. 7, revealing that the densification of the composite powder compact starts at lower temperatures during PECS, as compared to HP. Furthermore, the obtained shrinkage rate during PECS is higher compared to the one during HP.

Discussion

The previous paragraphs clearly indicated that a more homogeneous nanostructured composite material could be obtained using a high energetic bead milling procedure using small ceramic beads. Moreover, the intrinsic

nanostructure of the starting powders can be maintained in the densified composite material using a fast sintering method, a relatively low sintering temperature and short dwell time.

Besides the maintained nanostructure, a material with excellent fracture toughness can be obtained, as listed in Table 1, which is very unusual for nanocomposites. The fracture toughness of the different ZrO_2–$TiC_{0.5}N_{0.5}$ (60/40) materials is correlated with the $t \rightarrow m$ transformability of the Y-ZrO_2 matrix as shown in Fig. 8, unequivocally proving that transformation toughening is the main toughening mechanism. When the yttria content of the Y-ZrO_2 matrix is below 2 mol%, spontaneous transformation from the tetragonal to the monoclinic phase occurred, as confirmed by the XRD pattern of the polished surface of the ZrO_2–$TiC_{0.5}N_{0.5}$ (60/40) composite with a stabiliser content of 1.75 mol%. The spontaneous transformation is accompanied with a reduced density and inferior properties due to the presence of microcracks, as summarised in Table 1.

When the densification behaviour of a ZrO_2–TiCN (60/40) composite powder compact during HP and PECS is compared, it was observed that densification starts at a lower temperature and the maximum densification rate was higher in case of PECS. Assuming percolation type behaviour [23, 24] and homogeneously dispersed secondary TiCN phase particles inside the Y-ZrO_2 matrix, the maximum densification rate is obtained at temperatures below the theoretically calculated percolation temperature, as shown in Fig. 9. However, when the tool resistance, as calculated from the measured voltage and current using probes that are inserted in the electrodes of the PECS equipment as shown in Fig. 10a, is plotted as a function of the pyrometer temperature (Fig. 10b), the most distinct change in overall tool resistance is observed in the 775–1,050 °C region. This indicates that the sample already becomes electrically conductive before reaching the theoretical percolation limit assuming homogeneously dispersed spherical secondary phase particles. A similar type of behaviour has been observed in epoxy-carbon

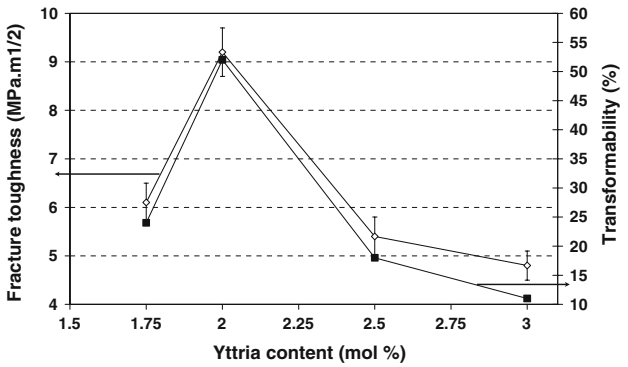

Fig. 8 Fracture toughness and ZrO_2 matrix transformability as a function of the yttria stabiliser content in ZrO_2–TiCN (60/40) composites, PECS for 2 min at 1,400 °C and 60 MPa

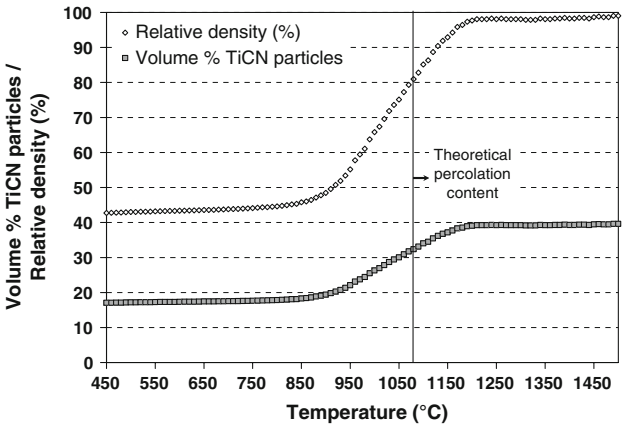

Fig. 9 Evolution of the relative density (◇) and volume per cent of electrically conductive TiCN particles (■) inside a sintering ZrO_2–$TiC_{0.5}N_{0.5}$ (60/40) composite powder compact as function of the PECS temperature. The solid vertical line indicates the theoretical percolation content in case of homogeneously dispersed spherical secondary phase particles in the Y-ZrO_2 matrix [24]

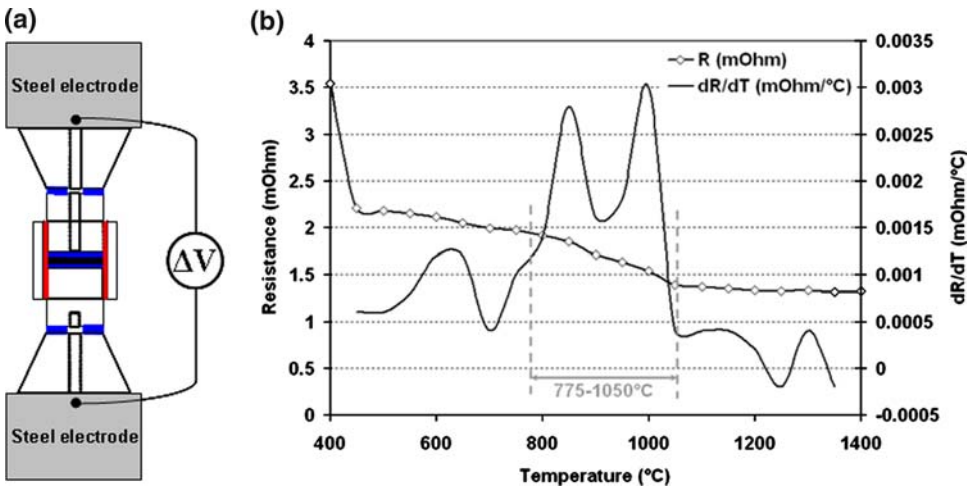

Fig. 10 Position of the voltage probes inside the steel electrodes (**a**) that were used to analytically calculate the Ohmic resistance of a PECS tool set-up throughout the sintering cycle, shown in Fig. 6a (**b**)

nanotube composites [25]. The exact reason for the low percolation threshold will be the subject of future research.

Conclusions

Nanostructured ZrO_2–TiCN (60/40) composites have been obtained by PECS at 1,400 °C for 2 min applying a pressure of 60 MPa. Due to the use of a high energetic bead milling procedure, the nanometer-sized (<100 nm) $TiC_{0.5}N_{0.5}$ particles were homogeneously dispersed in the Y-ZrO_2 matrix, and no distinct TiCN grain growth was observed. Since the fracture toughness of the composite could be controlled by adjusting the yttria stabiliser content in the Y-ZrO_2 matrix, nanocomposites with an excellent fracture toughness up to 9 MPa $m^{1/2}$ could be realised. The Young's modulus, Vickers hardness and 3-point bending strength were slightly higher than that of 2Y-TZP. Moreover, the material was electrically conductive and could be machined by EDM.

It is demonstrated that PECS offers advantages as compared to conventional HP, not only in terms of time gain, but also by enhancing the densification behaviour of electrically conductive materials. Furthermore, it was shown that percolation took place below the theoretically calculated threshold value, suggesting that an electrically conductive composite material could even be obtained with lower volume fractions of secondary phase particles.

Acknowledgements This work was performed within the framework of the Research Fund of K.U.Leuven under project GOA/08/007 and FWO project grant number 3E060133. K. Vanmeensel thanks the Fund for Scientific Research Flanders (FWO), S. Salehi thanks the Research Council of K.U.Leuven for a doctoral scholarship (DB/07/012) and A Laptev acknowledges the Research Council of K.U.Leuven for his research fellowship. The authors also acknowledge the support of the Belgian Federal Science Policy Office (BELSPO) through the NACER project (contract P2/00/07).

References

1. Garvie RC, Hannink RHJ, Pascoe RT (1975) Nature 258:703
2. Hannink RHJ, Kelly PM, Muddle BC (2000) J Am Ceram Soc 83:461
3. Basu B, Vleugels J, Van der Biest O (2002) Key Eng Mater 206–213:1177
4. Huang SG, Vanmeensel K, Van der Biest O, Vleugels J (2007) J Eur Ceram Soc 27:3269
5. Basu B, Vleugels J, Van der Biest O (2002) J Alloys Compd 334:200
6. Vleugels J, Van der Biest O (1999) J Am Ceram Soc 82:2717
7. Vanmeensel K, Sastry KY, Laptev A, Vleugels J, Van der Biest O (2005) Solid State Phenom 106:153
8. Salehi S, Van der Biest O, Vleugels J (2006) J Eur Ceram Soc 26(15):3173
9. Rul S, Lefevre-Schlick F, Capria E, Laurent C, Peigney A (2004) Acta Mater 52:1061
10. Jiang D, Van der Biest O, Vleugels J (2007) J Eur Ceram Soc 27:1247
11. Duan RG, Kuntz JD, Garay JE, Mukherjee AK (2004) Scripta Mater 50:1309
12. Kawano S, Takahashi J, Shimada S (2004) J Eur Ceram Soc 24:309
13. Mayo MJ (2000) Adv Eng Mater 2:409
14. Guo Z, Blugan G, Kirchner R, Reece M, Graule T, Kuebler J (2007) Ceram Int 33:1223
15. Kear BH, Colaizzi J, Mayo WE, Liao SC (2001) Scripta Mater 44:2065
16. Angerer P, Yu LG, Khor KA, Krumpel G (2004) Mater Sci Eng A 381:16
17. Nygren M, Shen Z (2003) Solid State Sci 5:125
18. Basu B, Vleugels J, Van der Biest O (2004) Mater Sci Eng A 380:215
19. Vanmeensel K, Laptev A, Hennicke J, Vleugels J, Van der Biest O (2005) Acta Mater 53:4379
20. Anstis GR, Chantikul P, Lawn BR, Marshall DB (1981) J Am Ceram Soc 64:533
21. Roebben G, Basu B, Vleugels J, Van Humbeeck J, Van der Biest O (2000) J Alloys Compd 310:284
22. Toraya H, Yoshimura M, Somiya S (1984) J Am Ceram Soc 67:C119
23. Bánhegyi G (1986) Colloid Polym Sci 264:1030
24. Vanmeensel K, Laptev A, Van der Biest O, Vleugels J (2007) Acta Mater 55:1401
25. Sandler JKW, Kirk JE, Kinloch IA, Shaffer MSP, Windle AH (2003) Polymer 44:5893